Applied and Computational Mechanics 16 (2022) 119–134

Applied and Computational Mechanics

Comparison of implicit time-discretization schemes for hybridized discontinuous Galerkin methods

T. Levý[a,*], G. May[b]

[a] *Department of Mechanics, Faculty of Applied Sciences, University of West Bohemia, Technická 8, 301 00 Plzeň, Czech Republic*
[b] *Aeronautics and Aerospace Department, von Karman Institute for Fluid Dynamics, Waterloosesteenweg 72, B-1640 Sint-Genesius-Rode, Belgium*

Received 19 September 2022; accepted 11 November 2022

Abstract

The present study is focused on the application of two families of implicit time-integration schemes for general time-dependent balance laws of convection-diffusion-reaction type discretized by a hybridized discontinuous Galerkin method in space, namely backward differentiation formulas (BDF) and diagonally implicit Runge-Kutta (DIRK) methods. Special attention is devoted to embedded DIRK methods, which allow the incorporation of time step size adaptation algorithms in order to keep the computational effort as low as possible. The properties of the numerical solution, such as its order of convergence, are investigated by means of suitably chosen test cases for a linear convection-diffusion-reaction equation and the nonlinear system of Navier-Stokes equations. For problems considered in this work, the DIRK methods prove to be superior to high-order BDF methods in terms of both stability and accuracy.

Keywords: hybridized discontinuous Galerkin method, time-dependent convection-diffusion-reaction problems, backward differentiation formulas, diagonally implicit Runge-Kutta method, time step size adaptation

1. Introduction

High-order methods are of great interest for problems of computational fluid dynamics (CFD) because of their potential in delivering higher accuracy of the numerical solution at a lower cost compared to conventional low-order methods. One such method is the hybridized discontinuous Galerkin (HDG) method [10,20,21], which benefits from having fewer globally coupled degrees of freedom (DOF) compared to the standard discontinuous Galerkin (DG) method [3, 4]. In this work, we are interested in further extension of the existing HDG solver, which has been developed for solving steady-state problems [29]. The main goal is to extend the solver for generic time-dependent balance laws of convection-diffusion-reaction type with emphasis on mathematical models arising in the field of CFD such as the systems of Euler and Navier-Stokes equations governing compressible fluid flow.

A lower number of globally coupled DOF compared to standard DG is especially beneficial for implicit time integration in which case large systems of linearized equations have to be solved in each time step. The hybridized formulation introduces a new variable, usually called λ, which is defined only on the faces of mesh elements. This procedure would usually lead to an increase in the total number of unknowns of the resulting system of equations. However, the method allows elimination of the primary variables and reformulation of the global system in

*Corresponding author. Tel.: +420 377 632 337, e-mail: levyto@kme.zcu.cz.
https://doi.org/10.24132/acm.2022.786

terms of λ only. The remaining DOF can then be recovered locally in an element-by-element fashion.

Applying the HDG method to an unsteady convection-diffusion-reaction equation leads to a system of differential-algebraic equations (DAEs) of index one representing a stiff problem [27]. Therefore, the use of explicit methods for time integration is impossible and one has to choose an appropriate implicit method for solving DAEs. In order to minimize the number of time steps needed to achieve the desired accuracy of the numerical solution at the final time of the simulation, we aim to use high-order methods also in time. Two families of methods are considered in this work. These are backward differentiation formulas (BDF) and diagonally implicit Runge-Kutta (DIRK) methods. DIRK methods are often designed such that they include an embedded method of lower order by which one can obtain another estimate of the numerical solution in a particular time step without additional computational effort. Based on the norm of the difference between these two solutions a time step control algorithm can be employed in order to keep the local error below a prescribed tolerance.

The contribution of this study lies in the comparison of herein considered time-integration methods on problems for linear convection-diffusion-reaction equations using suitably chosen manufactured solutions designed to verify the order of convergence of the numerical solution and other properties of a given method combined with the HDG discretization in space. Finally, laminar compressible flow past a circular cylinder governed by the nonlinear system of Navier-Stokes equations is studied in order to test the time step control algorithm for real fluid-flow problems.

2. Hybridized discontinuous Galerkin method for unsteady problems

2.1. Governing equations

We consider the time-dependent case of general convection-diffusion-reaction systems of equations defined on an open bounded domain $\Omega \in \mathbb{R}^d$, $d = 2$. These problems can be written in the form

$$\partial_t \boldsymbol{w} + \nabla \cdot [\boldsymbol{f}_c(\boldsymbol{w}) - \boldsymbol{f}_v(\boldsymbol{w}, \nabla \boldsymbol{w})] = \boldsymbol{s}(\boldsymbol{w}, \nabla \boldsymbol{w}) \tag{1}$$

together with appropriate initial and boundary conditions. Here, $\boldsymbol{w} \in \mathbb{R}^m$ is the vector of conservative variables, $\boldsymbol{f}_c : \mathbb{R}^m \to \mathbb{R}^{m \times d}$ is the convective flux, $\boldsymbol{f}_v : \mathbb{R}^m \times \mathbb{R}^{m \times d} \to \mathbb{R}^{m \times d}$ is the viscous flux and $\boldsymbol{s} : \mathbb{R}^m \times \mathbb{R}^{m \times d} \to \mathbb{R}^m$ is the source term.

Formulation (1) covers the scalar linear convection-diffusion-reaction equation with $\boldsymbol{f}_c = \boldsymbol{u}w$, where $\boldsymbol{u} \in [L^\infty(\Omega)]^d$ is the velocity vector field. Another specific example used throughout this study is the system of Navier-Stokes equations with $m = 4$ and

$$\boldsymbol{w} = \begin{pmatrix} \varrho \\ \varrho \boldsymbol{u} \\ E \end{pmatrix}, \quad \boldsymbol{f}_c = \begin{pmatrix} \varrho \boldsymbol{u}^T \\ \varrho \boldsymbol{u} \otimes \boldsymbol{u} + P \boldsymbol{I}_d \\ (E + P) \boldsymbol{u}^T \end{pmatrix}, \quad \boldsymbol{f}_v = \begin{pmatrix} 0 \\ \boldsymbol{\tau}_v \\ \boldsymbol{\tau}_v \cdot \boldsymbol{u} + k(\nabla \theta)^T \end{pmatrix}, \quad \boldsymbol{s} = \boldsymbol{0}, \tag{2}$$

where ϱ is the density, $\boldsymbol{u} = (u, v)^T$ is the fluid velocity vector, E is the total energy per unit volume, θ is the thermodynamic temperature, k is the thermal conductivity coefficient and $\boldsymbol{I}_d \in \mathbb{R}^{d \times d}$ is the identity matrix. The pressure P is related to the conservative variables by the equation of state of an ideal gas in the form

$$P = (\gamma - 1) \left(E - \frac{1}{2} \varrho |\boldsymbol{u}|_2^2 \right), \tag{3}$$

where γ is the ratio of specific heats and $\gamma = 1.4$ for air. For a Newtonian fluid, using the Stokes' hypothesis, the viscous stress tensor is defined as

$$\boldsymbol{\tau}_v = \mu \left[\nabla \boldsymbol{u} + (\nabla \boldsymbol{u})^T - \frac{2}{3}(\nabla \cdot \boldsymbol{u}) \boldsymbol{I}_d \right]. \tag{4}$$

Furthermore, we assume the dynamic viscosity to be a function of thermodynamic temperature determined by the Sutherland's law $\mu = C_1 \theta^{\frac{3}{2}}/(\theta + C_2)$ with $C_1 = 1.458 \times 10^{-6}\,\mathrm{kg}/(\mathrm{ms}\sqrt{\mathrm{K}})$ and $C_2 = 110.4\,\mathrm{K}$.

2.2. Semi-discrete formulation

Let the computational domain Ω be partitioned into a collection of nonoverlapping elements denoted by $\mathcal{T}_h$ such that $\Omega = \bigcup_{\kappa \in \mathcal{T}_h} \kappa$. For the element edges, two different kinds of sets are considered, which are element-oriented and edge-oriented. Let $\partial \mathcal{T}_h := \{\partial \kappa \backslash \partial \Omega : \kappa \in \mathcal{T}_h\}$ be the set of all edges of the elements, excluding the domain boundary. Next, we denote the set of all interior edges of $\mathcal{T}_h$ by $\mathcal{E}_h$. The boundary edges are contained in set $\mathcal{E}_h^{\partial}$.

Introducing an auxiliary variable $\boldsymbol{q}$, which represents the gradient of the solution, the balance law (1) can be rewritten as a first-order system of the form

$$\boldsymbol{q} - \nabla \boldsymbol{w} = \boldsymbol{0}, \tag{5}$$

$$\partial_t \boldsymbol{w} + \nabla \cdot [\boldsymbol{f}_c(\boldsymbol{w}) - \boldsymbol{f}_v(\boldsymbol{w}, \boldsymbol{q})] = \boldsymbol{s}(\boldsymbol{w}, \boldsymbol{q}). \tag{6}$$

In contrast to standard discontinuous Galerkin (DG) methods, the hybridized weak formulation is obtained by introduction of an additional unknown $\boldsymbol{\lambda}$, which represents the trace of the solution at the element edges. This procedure leads to a reduction of the globally coupled degrees of freedom compared to the DG method since it is possible to eliminate the primary variables by a static condensation process resulting in a formulation of the global problem in terms of $\boldsymbol{\lambda}$ only. In order to close the system of equations, the continuity of convective and diffusive numerical fluxes at the edges is enforced in the weak sense.

Let $\mathcal{P}^p(D)$ denote a set of polynomials of total degree at most p on some domain D. For the representation of the approximate solution $\mathbb{x}_h := (\boldsymbol{q}_h, \boldsymbol{w}_h, \boldsymbol{\lambda}_h)$, we consider the following approximation function spaces

$$\Sigma_h := \{\boldsymbol{\tau} \in \left[L^2(\Omega)\right]^{m \times d} : \boldsymbol{\tau}|_\kappa \in \left[\mathcal{P}^p(\kappa)\right]^{m \times d}, \forall \kappa \in \mathcal{T}_h\}, \tag{7}$$

$$V_h := \{\boldsymbol{v} \in \left[L^2(\Omega)\right]^{m} \quad : \boldsymbol{v}|_\kappa \in \left[\mathcal{P}^p(\kappa)\right]^{m}, \quad \forall \kappa \in \mathcal{T}_h\}, \tag{8}$$

$$\Lambda_h := \{\boldsymbol{\mu} \in \left[L^2(\mathcal{E}_h)\right]^{m} \quad : \boldsymbol{\mu}|_e \in \left[\mathcal{P}^p(e)\right]^{m}, \quad \forall e \in \mathcal{E}_h\}. \tag{9}$$

Functions $\boldsymbol{\tau} \in \Sigma_h$, $\boldsymbol{v} \in V_h$, and $\boldsymbol{\mu} \in \Lambda_h$ are piecewise polynomials of degree p, which can be discontinuous across element faces ($\boldsymbol{\tau}$ and $\boldsymbol{v}$) and vertices ($\boldsymbol{\mu}$), respectively.

The hybridized weak formulation of the system, consisting of the equations for the solution gradient $\boldsymbol{q}_h$, the solution itself $\boldsymbol{w}_h$ and its trace at the element edges $\boldsymbol{\lambda}_h$, has the following form: Find $\mathbb{x}_h \in \mathbb{X}_h := \Sigma_h \times V_h \times \Lambda_h$ such that

$$\begin{aligned}
0 &= \mathcal{N}(\mathbb{x}_h; \mathbb{y}_h) \\
&:= (\boldsymbol{q}_h, \boldsymbol{\tau}_h)_{\mathcal{T}_h} + (\boldsymbol{w}_h, \nabla \cdot \boldsymbol{\tau}_h)_{\mathcal{T}_h} - \langle \boldsymbol{\lambda}_h, \boldsymbol{\tau}_h \cdot \boldsymbol{n} \rangle_{\partial \mathcal{T}_h} \\
&\quad + (\partial_t \boldsymbol{w}_h, \boldsymbol{v}_h)_{\mathcal{T}_h} - (\boldsymbol{f}_{c,h} - \boldsymbol{f}_{v,h}, \nabla \boldsymbol{v}_h)_{\mathcal{T}_h} - (\boldsymbol{s}_h, \boldsymbol{v}_h)_{\mathcal{T}_h} + \left\langle \left(\widehat{\boldsymbol{f}}_c - \widehat{\boldsymbol{f}}_v \right) \cdot \boldsymbol{n}, \boldsymbol{v}_h \right\rangle_{\partial \mathcal{T}_h} \\
&\quad + \left\langle \left[\!\left[\widehat{\boldsymbol{f}}_c - \widehat{\boldsymbol{f}}_v \right]\!\right], \boldsymbol{\mu}_h \right\rangle_{\mathcal{E}_h} + \mathcal{N}_{h,\partial\Omega}(\boldsymbol{q}_h, \boldsymbol{w}_h; \boldsymbol{\tau}_h, \boldsymbol{v}_h)
\end{aligned} \tag{10}$$

holds for all $\mathbb{y}_h := (\boldsymbol{\tau}_h, \boldsymbol{v}_h, \boldsymbol{\mu}_h) \in \mathbb{X}_h$. Here, we have used the abbreviation $(\cdot,\cdot)$ and $\langle\cdot,\cdot\rangle$ to distinguish between element-oriented and edge-oriented inner products. The jump operator for a vector-valued function is defined as $[\![\boldsymbol{v}]\!] := \boldsymbol{v}^+ \cdot \boldsymbol{n} + \boldsymbol{v}^- \cdot \boldsymbol{n}^-$ where the signs $\pm$ correspond to elements κ^+ and κ^- separated by an edge. We choose convective and diffusive numerical fluxes corresponding to the Lax-Friedrichs flux and LDG flux [11], respectively, i.e.,

$$\widehat{\boldsymbol{f}}_c(\boldsymbol{\lambda}_h, \boldsymbol{w}_h) = \boldsymbol{f}_c(\boldsymbol{\lambda}_h) \cdot \boldsymbol{n} - \alpha_c \left(\boldsymbol{\lambda}_h - \boldsymbol{w}_h\right), \tag{11}$$

$$\widehat{\boldsymbol{f}}_v(\boldsymbol{\lambda}_h, \boldsymbol{w}_h, \boldsymbol{q}_h) = \boldsymbol{f}_v(\boldsymbol{\lambda}_h, \boldsymbol{q}_h) \cdot \boldsymbol{n} + \alpha_v \left(\boldsymbol{\lambda}_h - \boldsymbol{w}_h\right), \tag{12}$$

where we assume α_c and α_v to be constant scalar values.

The boundary conditions are incorporated into the scheme by evaluating the exact flux functions with a suitably chosen vector of conservative variables at the domain boundary $\boldsymbol{w}_{h,\partial\Omega}$ and its gradient $\boldsymbol{q}_{h,\partial\Omega}$ depending on a particular type of the boundary condition such that an adjoint-consistent scheme is retrieved [24],

$$\begin{aligned}\mathcal{N}_{h,\partial\Omega}(\boldsymbol{q}_h, \boldsymbol{w}_h; \boldsymbol{\tau}_h, \boldsymbol{v}_h) = {} & \langle \boldsymbol{w}_{h,\partial\Omega}(\boldsymbol{w}_h), \boldsymbol{\tau}_h \cdot \boldsymbol{n}\rangle_{\mathcal{E}_h^\partial} \\ & + \langle (\boldsymbol{f}_c(\boldsymbol{w}_{h,\partial\Omega}(\boldsymbol{w}_h)) - \boldsymbol{f}_v(\boldsymbol{w}_{h,\partial\Omega}(\boldsymbol{w}_h), \boldsymbol{q}_{h,\partial\Omega}(\boldsymbol{q}_h))) \cdot \boldsymbol{n}, \boldsymbol{v}_h\rangle_{\mathcal{E}_h^\partial}.\end{aligned} \tag{13}$$

2.3. Time integration

Now we focus on how to apply the time integration to the semi-discrete formulation. For this purpose, we rewrite the weak formulation (10) as: Find $\mathbb{x}_h \in \mathbb{X}_h$ such that

$$\mathcal{T}(\partial_t \mathbb{x}_h; \mathbb{y}_h) + \mathcal{N}(\mathbb{x}_h; \mathbb{y}_h) = 0 \quad \forall \mathbb{y}_h \in \mathbb{X}_h, \tag{14}$$

where we split the term with the time derivative from the other terms and $\mathcal{T}(\partial_t \mathbb{x}_h; \mathbb{y}_h) = (\partial_t \boldsymbol{w}_h, \boldsymbol{v}_h)_{\mathcal{T}_h}$. Since only the time derivative of variable $\boldsymbol{w}_h$ appears in (14), it constitutes a set of differential-algebraic equations (DAEs) and, hence, the classical approach of using method of lines with some explicit scheme cannot be used. Instead, one has to choose an appropriate implicit method for solving DAEs. Along with the HDG method, backward differentiation formulas (BDF) and diagonally implicit Runge-Kutta (DIRK) methods have been first applied by Nguyen et al. [20, 21]. For the case of BDF methods up to order three, see also the work of Schütz et al. [25].

Applying a general k-step BDF method to formulation (14) in order to find the solution at time t^{n+k} results in

$$\frac{\alpha_k}{\beta_0 \Delta t}\mathcal{T}(\mathbb{x}_h^{n+k}; \mathbb{y}_h) + \mathcal{N}(\mathbb{x}_h^{n+k}; \mathbb{y}_h) = -\sum_{j=0}^{k-1} \frac{\alpha_j}{\beta_0 \Delta t}\mathcal{T}(\mathbb{x}_h^{n+j}; \mathbb{y}_h) \quad \forall \mathbb{y}_h \in \mathbb{X}_h, \tag{15}$$

which needs to be solved in each time step n. The coefficients β_0 and $\alpha_j, j = 0, \ldots, k$ can be found in [27]. Note that BDF methods are stable only for $k \leq 6$ and, moreover, they are A-stable only for $k \leq 2$ which can lead to instability for stiff problems when using BDF of higher order. Furthermore, BDF methods need a suitable starting procedure in order to generate numerical solutions in the first $(k-1)$ time steps. In this work, unless the exact solution of a particular problem is known, we use the DIRK methods at the beginning of the computation.

The solution in time step $(n+1)$ can be determined from the solution at time step n using an s-stage DIRK method by solving

$$\mathcal{T}(\mathbb{x}_h^{n+1}; \mathbb{y}_h) = \mathcal{T}(\mathbb{x}_h^{n}; \mathbb{y}_h) - \Delta t \sum_{i=1}^{s} b_i \mathcal{N}(\mathbb{x}_h^{n,i}; \mathbb{y}_h) \quad \forall \mathbb{y}_h \in \mathbb{X}_h. \tag{16}$$

The intermediate solutions $\mathbb{x}_h^{n,i}, i = 1, \ldots, s$ have to be obtained by solving

$$\frac{1}{a_{ii}\Delta t}\mathcal{T}(\mathbb{x}_h^{n,i}; \mathbb{y}_h) + \mathcal{N}(\mathbb{x}_h^{n,i}; \mathbb{y}_h) = \frac{1}{a_{ii}\Delta t}\mathcal{T}(\mathbb{x}_h^{n}; \mathbb{y}_h) - \sum_{j=1}^{i-1} \frac{a_{ij}}{a_{ii}}\mathcal{N}(\mathbb{x}_h^{n,j}; \mathbb{y}_h) \quad \forall \mathbb{y}_h \in \mathbb{X}_h \quad (17)$$

in each stage of the DIRK method, where $t^{n,i} = t^n + c_i\Delta t$. The coefficients a_{ij}, b_i, and c_i determine the order of consistency q of the given DIRK scheme and are usually represented by a table as shown in Table 1. From now on, a DIRK method of order q and number of stages s will be denoted by DIRK(s, q).

Table 1. Butcher table of an embedded DIRK method

c_1	a_{11}			
c_2	a_{21}	a_{22}		
$\vdots$	$\vdots$	$\vdots$	$\ddots$	
c_s	a_{s1}	a_{s2}	$\cdots$	a_{ss}
	b_1	b_2	$\cdots$	b_s
	$\widehat{b}_1$	$\widehat{b}_2$	$\cdots$	$\widehat{b}_s$

Note that once the intermediate solutions are known, the final step (16) is an explicit operation. However, we are particularly interested in the subset of so-called singly diagonally implicit Runge-Kutta (SDIRK) methods, which satisfy $a_{ii} = \gamma, i = 1, \ldots, s$. In addition, the *stiffly accurate* methods satisfy $a_{sj} = b_j, j = 1, \ldots, s$ and, hence, the numerical solution in the next time step is identical to the last-stage intermediate solution, such that the final step (16) is not needed. In this work, three stiffly accurate SDIRK methods are considered. In particular, we use the two-stage second-order DIRK(2, 2) method of Alexander [1], the three-stage third-order DIRK(3, 3) of Cash [9], and the five-stage fourth-order DIRK(5, 4) method of Hairer and Wanner [27]. The full Butcher tables of these methods are given by Tables 2–4.

Table 2. Butcher table of DIRK(2, 2) method

γ	γ	
1	$1-\gamma$	γ
1	$1-\gamma$	γ

$$\gamma = \frac{1}{2}\left(2 - \sqrt{2}\right)$$

Table 3. Butcher table of DIRK(3, 3) method, $\gamma = 0.435\,866\,521\,508\,458$

γ	γ		
τ_2	$\tau_2 - \gamma$	γ	
1	b_1	b_2	γ
	b_1	b_2	γ
	c_1	c_2	

$$\tau_2 = \frac{\gamma^2 - \frac{3}{2}\gamma + \frac{1}{3}}{\gamma^2 - 2\gamma + \frac{1}{2}} \qquad b_1 = \frac{\frac{1}{2}\tau_2 - \frac{1}{6}}{(\tau_2 - \gamma)(1 - \gamma)} \qquad c_1 = \frac{\tau_2 - \frac{1}{2}}{\tau_2 - \gamma}$$

$$b_2 = \frac{\frac{1}{2}\gamma - \frac{1}{6}}{(\gamma - \tau_2)(1 - \tau_2)} \qquad c_2 = \frac{\gamma - \frac{1}{2}}{\gamma - \tau_2}$$

Table 4. Butcher table of DIRK(5, 4) method

$\frac{1}{4}$	$\frac{1}{4}$				
$\frac{3}{4}$	$\frac{1}{2}$	$\frac{1}{4}$			
$\frac{11}{20}$	$\frac{17}{50}$	$-\frac{1}{25}$	$\frac{1}{4}$		
$\frac{1}{2}$	$\frac{371}{1360}$	$-\frac{137}{2720}$	$\frac{15}{544}$	$\frac{1}{4}$	
1	$\frac{25}{24}$	$-\frac{49}{48}$	$\frac{125}{16}$	$-\frac{85}{12}$	$\frac{1}{4}$
	$\frac{25}{24}$	$-\frac{49}{48}$	$\frac{125}{16}$	$-\frac{85}{12}$	$\frac{1}{4}$
	$\frac{59}{48}$	$-\frac{17}{96}$	$\frac{225}{32}$	$-\frac{85}{12}$	

The resulting systems of (possibly) nonlinear equations (15) and (17) are solved by a damped Newton method in each time step for the case of BDF methods and in each stage of the DIRK method, respectively.

Application of DIRK-type methods to initial-boundary value problems can sometimes lead to so-called *order reduction*. The same phenomenon also appears in the numerical solution of some stiff problems for DAEs in which case the global convergence rate is lower than the order of the method [27]. In such situation, the observed convergence rate is related to the stage order r of the method.

For semi-discretized PDEs, which is precisely our case, the order reduction appears due to the presence of boundaries of the spatial domain and the interaction between the boundary conditions and the low-stage order information. The amount of the observed order reduction depends on a particular problem and the global convergence rate is usually equal to the minimum of the classical order of the method q and its stage order r plus some constant [16].

One of the earliest studies of this phenomenon is [26], where third- and fourth-order DIRK methods are applied to the time-dependent Burgers' and heat equation with either homogeneous or inhomogeneous Dirichlet boundary conditions discretized by finite differences. In the inhomogeneous case, the convergence rates are of order $(r + 1)$, while for the homogeneous boundary conditions only the convergence of the fourth-order DIRK method is slightly affected and the third-order method preserves the expected order of accuracy.

Some remedy to avoid these phenomena is indicated in the work of Calvo [8] or Alonso-Mallo [2]. A promising approach for overcoming order reduction is studied in recent works [23] and [17]. The authors suggest two ways to address this phenomenon, either modified boundary conditions or additional order conditions for the DIRK coefficients. In the latter case, they introduce the concept of *weak stage order*. In particular, [17] introduces three stiffly accurate L-stable SDIRK methods of weak stage orders two and three. These are third-order four-stage and fourth-order six-stage methods. As we have also encountered the order reduction for some test problems, we, therefore, adopt the methods with weak stage order three, hereafter referred to as DIRK(4, 3) and DIRK(6, 4).

One of the main advantages of one-step methods is that the size of the time step Δt can be changed between time steps without modification of the scheme. Additionally, Runge-Kutta methods are often equipped with an additional set of coefficients $\widehat{b}_j, j = 1, \ldots, s$, which are used to determine a second solution, usually of lower order, by replacing the coefficients b_i in (16). Such a method is then called embedded and can be used for error estimation after one

time step. The time step size then can be adjusted accordingly in order to achieve some specified error bound.

Let w_h^{n+1} and $\widehat{w}_h^{n+1}$ represent the numerical solution obtained by a DIRK method of order q in time step $(n+1)$ and the corresponding numerical solution of order $\widehat{q}$ given by the embedded formula. For the embedded methods, we consider DIRK(3, 3) and DIRK(5, 4), we have $\widehat{q} = q - 1$. The local error estimate after one time step can be written as

$$\mathcal{E} = \|w_h^{n+1} - \widehat{w}_h^{n+1}\|_2. \tag{18}$$

The numerical solution w_h^{n+1} will be accepted only if $\mathcal{E} \leq \texttt{Tol}$, where $\texttt{Tol}$ is defined by the user. In this study, we compute the new time step size Δt^{n+1} using the formula proposed by Hairer and Wanner in [14]

$$\Delta t^{n+1} = \Delta t^n \min\left\{ f_{\max}, \max\left[f_{\min}, f_{\text{safety}} \left(\frac{\mathcal{E}}{\texttt{Tol}} \right)^{-1/q} \right] \right\}, \tag{19}$$

where $f_{\max} = 5$, $f_{\min} = 0.2$ and

$$f_{\text{safety}} = 0.9 \, \frac{2n_{\text{it}}^{\max} + 1}{2n_{\text{it}}^{\max} + 2n_{\text{it}}} \tag{20}$$

with $n_{\text{it}}^{\max}$ and n_{it} being the prescribed maximum number of Newton iterations and maximum of actually performed Newton iterations over all stages, respectively. Moreover, the time step size is finally selected such that $\Delta t_{\min} \leq \Delta t^{n+1} \leq \Delta t_{\max}$.

The complete algorithm is as follows: If $\mathcal{E} \leq \texttt{Tol}$ holds, the time step size is accepted and the numerical solution is advanced in time with w_h^{n+1} and a new time step size Δt^{n+1} given by (19). Otherwise, the time step size is rejected and the computation of the time step is repeated with the time step size Δt^{n+1}.

3. Numerical results

3.1. Rotating Gaussian

First, we investigate a test case for the scalar linear convection-diffusion equation, which has been studied by Nguyen et al. in [20]. This example involves the rotational transport of a two-dimensional Gaussian pulse inside the domain $\Omega = [-0.5, 0.5]^2$. The velocity field is given by $\boldsymbol{u} = (-4y, 4x)$, and the final time of the simulation is $T = \pi/4$, which corresponds to a one-half rotation of the pulse in counterclockwise direction.

The exact solution for this problem is given by

$$w(x, y, t) = \frac{2\sigma^2}{2\sigma^2 + 4\varepsilon t} \exp\left[-\frac{(\widehat{x} - x_c)^2 + (\widehat{y} - y_c)^2}{2\sigma^2 + 4\varepsilon t} \right], \tag{21}$$

where

$$\widehat{x} = x\cos(4t) + y\sin(4t), \qquad \widehat{y} = -x\sin(4t) + y\cos(4t). \tag{22}$$

The initial center of the pulse is chosen to be $(x_c, y_x) = (-0.1, 0)$ and the standard deviation of the Gaussian distribution is set to $\sigma = 0.1$. Furthermore, we consider two different values for the diffusivity constant, $\varepsilon = 0.01$ and $\varepsilon = 0.001$. Dirichlet boundary conditions, deduced from the exact solution, are applied at the domain boundary.

By means of this particular test case, we would like to verify that the temporal convergence properties of the numerical solution are preserved for all considered time-marching methods. The numerical solution is computed numerous times with successively halved but fixed time step size Δt starting with $\Delta t = T/8$. For the representation of the solution on each mesh element, polynomials of degree $p = q + 1$ are assumed, where q is the design order of a particular time-integration method. Moreover, the mesh size is also successively halved in both spatial directions such that the ratio of time step size and the mesh size is kept constant. Based on the numerical experiments, this choice is sufficient for the spatial error to be enough such that the overall error is governed strictly by the temporal discretization error.

The results for the case of BDF methods are presented in Fig. 1a–b. One can see that up to BDF of order five, the numerical order of convergence corresponds to the theoretical order for both $\varepsilon = 0.01$ and $\varepsilon = 0.001$. Even in this linear problem, oscillations arise for the case

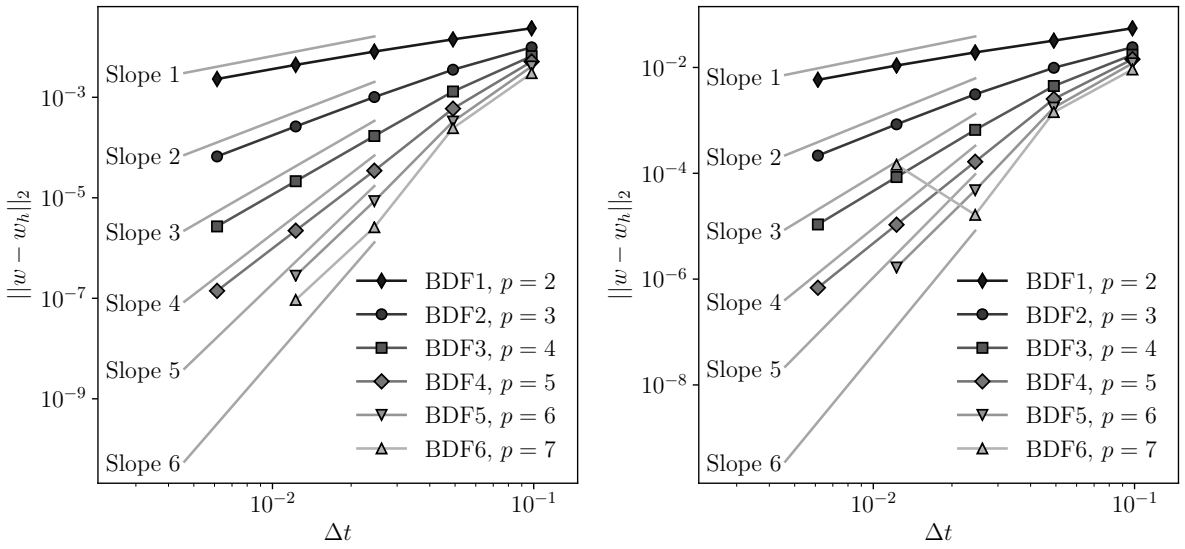

(a) BDF, $\varepsilon = 0.01$

(b) BDF, $\varepsilon = 0.001$

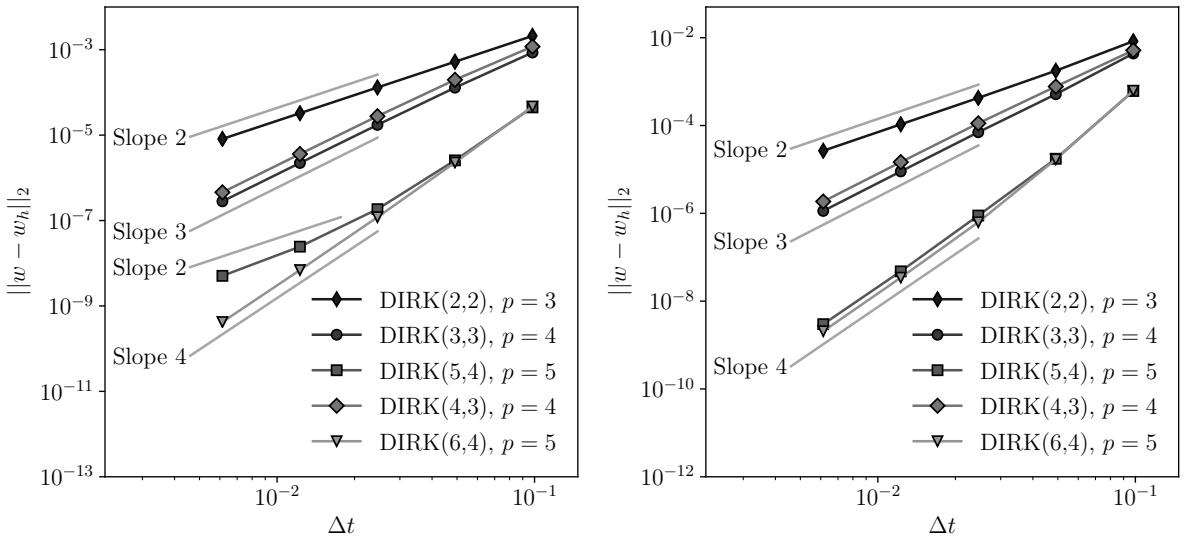

(c) DIRK, $\varepsilon = 0.01$

(d) DIRK, $\varepsilon = 0.001$

Fig. 1. Convergence study for the rotating Gaussian test case

of BDF6 in the bottom part of the domain as the time step size is decreased and, hence, the convergence rate fails to match the theoretical one in the asymptotic regime. In practice, due to weaker stability properties of the BDFk method with $k > 2$, these methods are rarely used for problems related to fluid dynamics [5]. Analysis of this phenomenon has been done in [6, 7], where the authors introduce BDF-ADI (Alternating Direction Implicit) methods as a remedy to this issue.

According to Fig. 1d, the numerical solution is qth-order accurate in time for all considered DIRK(s, q) methods and $\varepsilon = 0.001$. The same situation occurs for $\varepsilon = 0.01$ depicted in Fig. 1c except for the DIRK$(5, 4)$ method. In this case, as the time step size is decreased, the convergence of the numerical solution deteriorates from the expected behavior and second-order convergence is achieved. This is in complete agreement with the order reduction observed by Verwer [26] since the stage order of DIRK$(5, 4)$ is $r = 1$ as discussed in Section 2.3. Notice that the DIRK$(6, 4)$ method, which has weak stage order three, preserves the fourth-order convergence of numerical solution and does not suffer from order reduction.

3.2. Sine wave

Since the DIRK$(6, 4)$ method, Fig. 1c, reports expected convergence rate, the problem is not on the side of the implementation of boundary conditions. Hence, we would like to show the the order reduction seen for DIRK$(5, 4)$ is indeed related to the presence of the boundary of the computational domain.

Let us assume a solution of linear convection-diffusion-reaction equation, which is periodic on the unit square $\Omega = [-0.5, 0.5]^2$ and $\boldsymbol{u} = (1, 1)$. Let the manufactured solution have the form of a 2D sine wave, which travels diagonally through the domain and decays in time with respect to the diffusivity constant $\varepsilon = 0.01$,

$$w = \sin\left[2\pi\left(x - t\right)\right] \sin\left[2\pi\left(y - t\right)\right] \exp\left(-\varepsilon t\right). \tag{23}$$

The corresponding source term is given by

$$s = \varepsilon\left(8\pi^2 - 1\right) \sin\left[2\pi\left(x - t\right)\right] \sin\left[2\pi\left(y - t\right)\right] \exp\left(-\varepsilon t\right). \tag{24}$$

A triangular mesh with 512 elements and $p = 5$ polynomials are used to perform the temporal convergence study measured at final time $T = 1$ starting with time step size $\Delta t = 0.1$.

First, we set the Dirichlet boundary conditions deduced from the exact solution as in the rotating Gaussian test case. In Fig. 2a, we again observe the order reduction for the DIRK$(5, 4)$ method such that the order of convergence in the asymptotic regime corresponds to $(r + 1)$, i.e., second order. Since the exact solution is periodic in space, we can reformulate the problem by assuming periodic boundary conditions. The numerical solution of both problems then should be equivalent. However, according to Fig. 2b, this is not the case in terms of convergence and the theoretical orders of convergence are reached for all DIRK methods including DIRK$(5, 4)$.

3.3. Variable time step size

In order to analyze the behavior of the time step size control algorithm, we assume a manufactured solution, whose time scale is changing over time. Let the solution of a linear convection-diffusion-reaction equation be given by a sine wave on the unit square $\Omega = [0, 1]$, whose amplitude depends on the time variable t in a special way

$$w = \sin\left(\pi x\right) \sin\left(\pi y\right) \cos\left[12\pi t + \pi \sin\left(2\pi t\right)\right]. \tag{25}$$

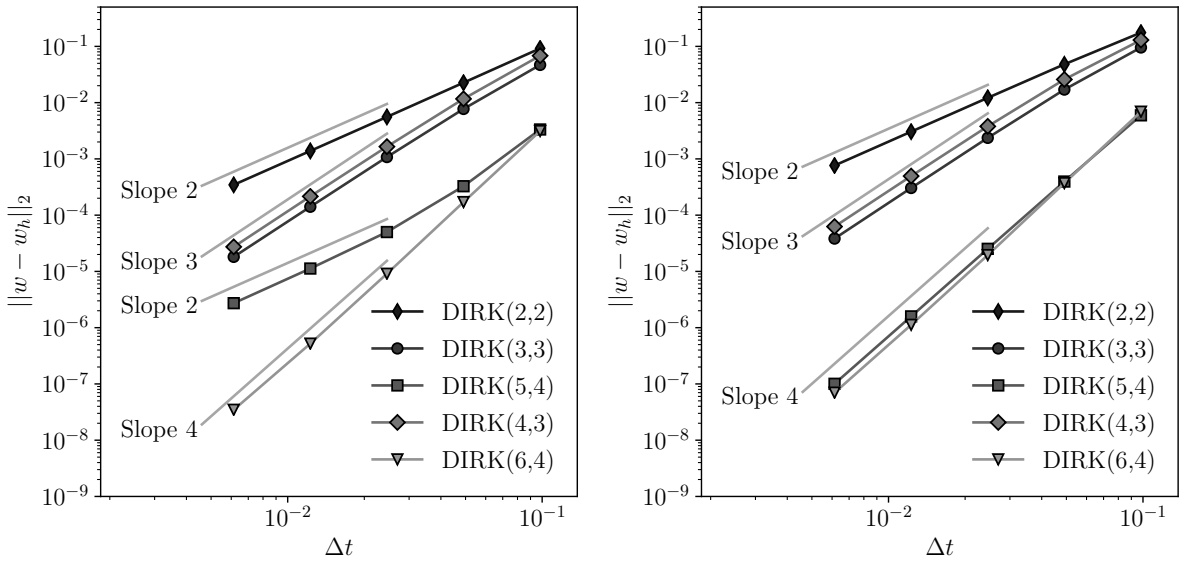

(a) Dirichlet boundary conditions

(b) Periodic boundary conditions

Fig. 2. Convergence study for the sine wave test case with two types of boundary conditions, $\varepsilon = 0.01$

The amplitude takes the form of a compound goniometric function of time such that the frequency of this function decreases on time interval $(0, 0.5)$ and increases on $(0.5, 1)$ in the opposite way. The exact solution at center point $\boldsymbol{x}_c = (0.5, 0.5)$ of the domain is plotted in the upper graph of Fig. 3. The reason for using this solution to analyze the time step adaptation algorithm is that the time step size should be adjusted according to the local slope of the solution in order for the estimated error to satisfy the prescribed tolerance. We should, therefore, observe a gradual increase of the time step size up to $t = 0.5$ and a gradual decrease in an almost symmetrical way towards $t = 1$.

The source term is derived in the following form:

$$s = \pi \cos(\xi)\big(c_x s_y + s_x c_y + 2\pi\varepsilon s_x s_y\big) - 2\pi \sin(\xi)\left[6 + \pi\cos(2\pi t)\right] s_x s_y, \tag{26}$$

where

$$\begin{aligned} s_x &= \sin(\pi x), & c_x &= \cos(\pi x), \\ s_y &= \sin(\pi y), & c_y &= \cos(\pi y), \end{aligned} \qquad \xi = 12\pi t + \pi \sin(2\pi t). \tag{27}$$

Next, we set $\varepsilon = 0.05$ and we use a triangular mesh with 800 elements together with $p = 3$ polynomials. Here, we study the effect of the absolute tolerance `Tol`, which is defined by the user. Homogeneous Dirichlet boundary conditions are assumed at the boundaries of the domain Ω and, hence, the order reduction of DIRK methods is avoided. For every case, we set the initial time step size to $\Delta t^0 = 0.01$ and $\Delta t_{\min} = 10^{-13}$, $\Delta t_{\max} = 1$ to fully examine the adaptation algorithm.

The evolution of time step size and L^2-error norm of the numerical solution are depicted in Fig. 3 for the case $\texttt{Tol} = 10^{-5}$. The black crosses represent the situation for DIRK(5, 4), where the time step is rejected and recomputed with a smaller time step size Δt. In the case of DIRK(3, 3), the time step is rejected only two times right at the start of the computation. The steep decrease of Δt at the end of the simulation is introduced in order to accurately reach the final time $T = 1$.

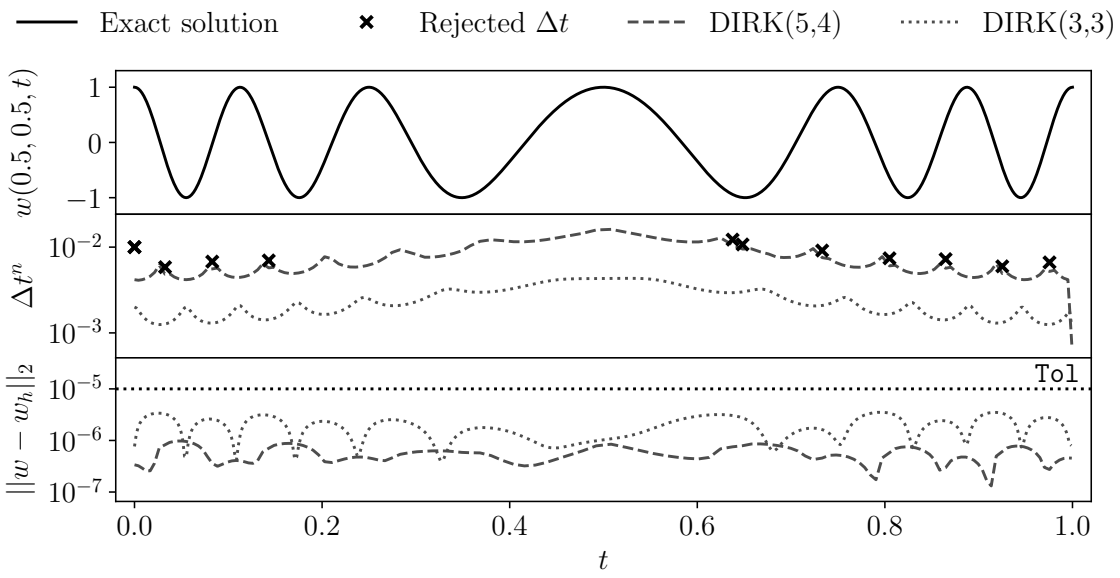

Fig. 3. Time step size adaptation, $\texttt{Tol} = 10^{-5}$

3.4. Flow past a circular cylinder

The last test case is a viscous laminar flow over a circular cylinder governed by the system of Navier-Stokes equations. The freestream conditions correspond to zero angle of attack, Mach number $\mathrm{Ma} = 0.2$ and Reynolds number $\mathrm{Re} = 100$ based on the cylinder diameter of unit length. Under these conditions, vortices are periodically shed from lower and upper parts of the cylinder surface and form the famous von Karman vortex street in the wake of the cylinder. Since the exact solution for this case is not known, the analysis will be rather qualitative and the achieved results will be compared to data of other authors by means of drag and lift coefficients of the cylinder C_D and C_L.

No-slip boundary condition is prescribed on the surface of the cylinder. The outer domain boundaries extend to 20 units away from the center of the cylinder and characteristic far-field boundary conditions are assumed. The size of the domain has been determined such that its further enlargement does not lead to a significant change in the mean value of the drag coefficient obtained from the developed flow field.

The computational mesh depicted in Fig. 4 consists of approximately 4 000 triangular elements and it is refined along the cylinder surface to appropriately resolve the boundary layer, as well as in the wake region to capture the vortex shedding. In order to test the time integration methods, we use $p = 4$ polynomials to represent the solution on a single element and the initial conditions are taken from the freestream values of the conservative variables. Thus, the vortex shedding starts to be fully developed and periodic in the time interval $t = (400, 700)$ depending on the size of the time step. Hence, we assume the final (non-dimensional) time of the computation $T = 1\,000$. Contours of vorticity magnitude $|\partial_x v - \partial_y u|$ at the final time are shown in Fig. 5.

We solve the problem using BDF2 and second-, third- and fourth-order DIRK methods of stage order one with three temporal refinements using a fixed time step size, namely $\Delta t = 2$, $1, 0.5$. Note that BDFk methods with $k > 2$ are not stable for this particular test case. The results obtained by each time-integration method are analyzed on the time interval $[800, 1\,000]$,

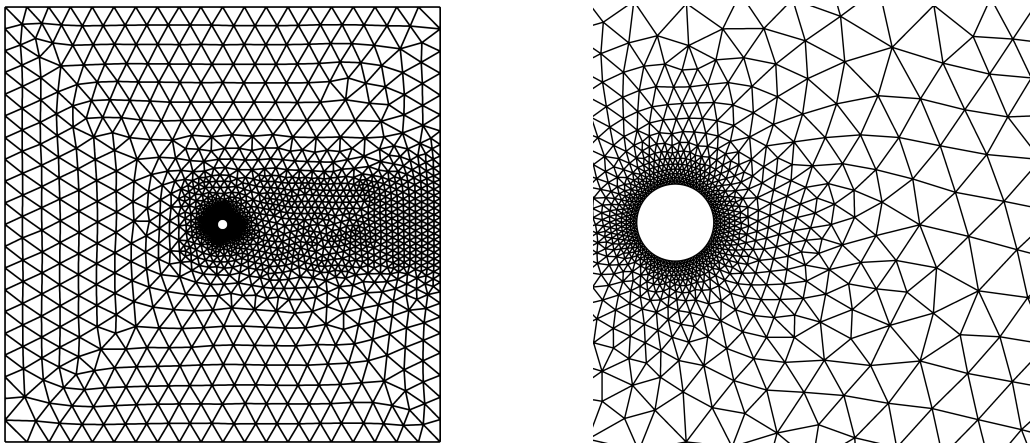

(a) Overall view (b) Detail in the vicinity of the cylinder

Fig. 4. Triangulation of the domain for flow past cylinder test case

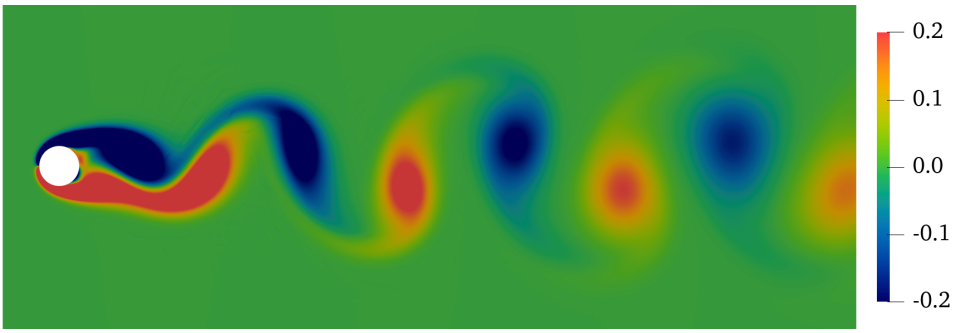

Fig. 5. Instaneous vorticity contours at $t = 1\,000$

which roughly corresponds to 8 periods in lift coefficient and 16 periods in drag coefficient. The mean drag coefficient $\overline{C_D}$, deviation from the mean of both drag and lift coefficients C'_D, C'_L and the Strouhal number $\mathrm{St} = fL/u_\infty$ are compared with results available in the literature, listed in Table 5. Here, f is the vortex shedding frequency, which is deduced from the Fourier transform of the periodic behavior of the lift coefficient C_L. Note that the results of Franciolini et al. [13] and Liang et al. [18] are obtained by solving the system of Navier-Stokes equations describing the flow of a compressible fluid with $\mathrm{Ma} = 0.2$ as in our case, while Ding et al. [12], Kang [15] and Meneghini et al. [19] assumed incompressible fluid flow. The result of Williamson [28] is measured by experiment.

The last tests are related to the embedded DIRK methods. The time step control algorithm is used with three different values of $\texttt{Tol} = 10^{-m}$ with $m = 3, 4, 5$, while the spatial discretization remains the same as before. We set $\Delta t_{\min} = 0.01$ and $\Delta t_{\max} = 5$. The lower bound is chosen in order to prevent the time step size to become extremely small during the initial phase when the boundary layer evolves. On the other hand, a reasonable upper bound has to be set for Δt to avoid obtaining a steady solution. The initial time step size Δt^0 is set to 1 which results in a few rejected time steps at the beginning of the computation.

The time step adaptation algorithm is analyzed in Table 6. Besides the cumulative number of Newton steps, we list also the overall number of GMRES iterations needed to drop the relative residual of the linearized system to 10^{-7} in each Newton iteration. One can see that even though

Table 5. Comparison of results from other authors and present results for flow past a cylinder at $\mathrm{Re} = 100$

	Δt	$\overline{C_D}$	C'_D	C'_L	St
Franciolini et al. [13]	–	1.352 8	–	–	0.164 1
Liang et al. [18]	–	1.365	0.008 6	0.232	0.164
Ding et al. [12]	–	1.35	0.01	0.287	0.166
Kang [15]	–	1.33	–	0.32	0.165
Meneghini et al. [19]	–	1.37	–	–	0.165
Williamson [28]	–	–	–	–	0.164
BDF2	2.0	1.332 3	0.006 2	0.260 9	0.150 8
	1.0	1.364 1	0.009 4	0.309 6	0.161 7
	0.5	1.364 6	0.009 4	0.328 6	0.164 6
DIRK(2, 2)	2.0	1.363 9	0.010 5	0.322 9	0.163 9
	1.0	1.369 8	0.009 7	0.333 5	0.165 1
	0.5	1.369 8	0.009 8	0.333 2	0.165 6
DIRK(3, 3)	2.0	1.363 8	0.009 2	0.320 7	0.164 6
	1.0	1.368 9	0.009 8	0.331 3	0.165 3
	0.5	1.369 6	0.009 9	0.332 6	0.165 6
DIRK(5, 4)	2.0	1.369 8	0.001 0	0.331 1	0.165 6
	1.0	1.369 8	0.009 9	0.332 9	0.165 6
	0.5	1.370 0	0.009 6	0.325 0	0.165 6

Table 6. The effect of `Tol` for flow past cylinder at $\mathrm{Re} = 100$

	`Tol`	Accepted time steps	Rejected time steps	$\overline{\Delta t}$	Newton steps	GMRES iterations	$\overline{C_D}$
DIRK(3, 3)	10^{-3}	314	2	3.18	3 649	42 616	1.349 7
	10^{-4}	813	2	1.23	9 214	71 925	1.368 7
	10^{-5}	1 888	2	0.47	18 398	93 913	1.369 8
DIRK(5, 4)	10^{-3}	320	3	3.13	6 416	62 376	1.368 7
	10^{-4}	605	2	1.65	11 092	77 409	1.369 9
	10^{-5}	1 073	4	0.93	19 221	104 560	1.369 9

the DIRK(5, 4) method results in higher mean time step size and, hence, a smaller number of time steps, the number of Newton steps is still higher than for DIRK(3, 3) and it is, therefore, more computationally demanding. However, the mean drag coefficient is well behaved already with $\texttt{Tol} = 10^{-4}$, while $\texttt{Tol} = 10^{-5}$ is needed for DIRK(3, 3) to reach the same value.

The evolution of time step size is plotted in Fig. 6. We can see that once the boundary layer is evolved, the time step size starts to gradually grow to $\Delta t^n = \Delta t_{\max}$, which is followed by a gradual decrease around $t = 300$. The detailed view shows the history of Δt^n on the time interval $[800, 1\,000]$, where the behavior more or less regularly follows the periodic nature of the flow.

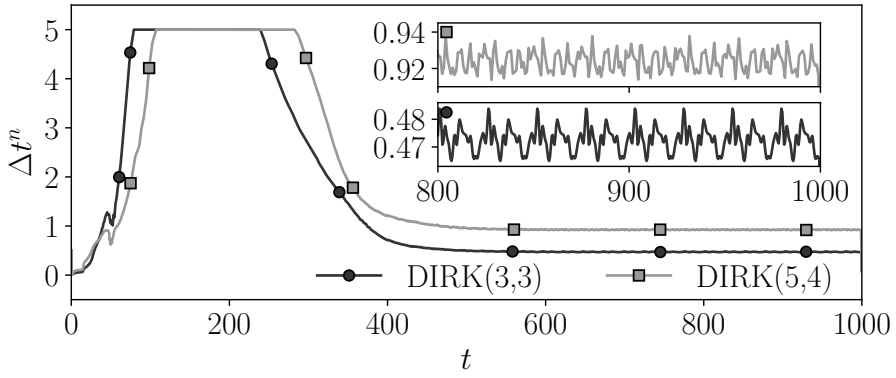

Fig. 6. Time step evolution of embedded DIRK methods with $\texttt{Tol} = 10^{-5}$

4. Conclusions

In the present paper, the HDG method was extended for time-dependent balance laws using two families of time-integration schemes, namely backward differentiation formulas and diagonally implicit Runge-Kutta methods.

We have seen that high-order BDF methods with $k > 2$ steps fail to provide reliable solutions for problems of practical importance due to their weaker stability properties. On the other hand, both BDF1 and BDF2 can be safely coupled with HDG discretization. Being only first- and second-order accurate, respectively, one may need to use a sufficiently small time step size if the temporal resolution is of great interest for a particular application.

In such situations, better accuracy can be achieved using DIRK methods, which come at the price of higher computational complexity since the nonlinear system of equations has to be solved multiple times during a single time step, depending on the number of Runge-Kutta stages of a given method. Although the DIRK methods perform very well in terms of stability, the test cases have shown that there can also be a mismatch in the observed order when solving initial-boundary value problems for PDEs. The order reduction phenomenon can cause the loss of advantages over lower-order BDF methods in cases, where the boundary conditions depend strongly on the solution itself or explicitly on time.

Since this phenomenon depends on the stage order of the DIRK method, a remedy to this problem has been proposed by using high weak stage order methods. We have shown that with DIRK$(4, 3)$ and DIRK$(6, 4)$ introduced in [17], the order reduction can be avoided for the test cases investigated in this work. However, these methods have an increased number of stages and, hence, the use of these methods is recommended only in situations, where the boundary conditions can have a significant impact on the solution accuracy. A preliminary assessment of such situations is of course not trivial and may require some numerical tests.

The other advantage of DIRK methods lies in using time step size adaptation based on the evolution of the solution itself. The embedded DIRK methods can easily outperform the fixed time step solution approach in terms of work needed to reach a specified error tolerance as seen in the flow past cylinder test case.

Ongoing work is focused on the coupling of the solution of time-dependent problems with the anisotropic mesh adaptation, which has been developed for steady equations [22]. The primary goal is to properly resolve the shock waves or regions of high solution gradients that are present in the flow field.

Acknowledgements

The work was supported from ERDF under project Research Cooperation for Higher Efficiency and Reliability of Blade Machines (LoStr) No. CZ.02.1.01/0.0/0.0/16_0008389 and the project SGS-2022-008.

References

[1] Alexander, R., Diagonally implicit Runge–Kutta methods for stiff O.D.E.'s, SIAM Journal on Numerical Analysis 14 (6) (1977) 1006–1021. https://doi.org/10.1137/0714068

[2] Alonso-Mallo, I., Cano, B., Avoiding order reduction of Runge-Kutta discretizations for linear time-dependent parabolic problems, BIT Numerical Mathematics 44 (1) (2004) 1–20. https://doi.org/10.1023/B:BITN.0000025087.83146.33

[3] Arnold, D., Brezzi, F., Cockburn, B., Marini, D., Unified analysis of discontinuous Galerkin methods for elliptic problems, SIAM Journal on Numerical Analysis 39 (2002) 1749–1779. https://doi.org/10.1137/S0036142901384162

[4] Bassi, F., Crivellini, A., Rebay, S., Savini, M., Discontinuous Galerkin solution of the Reynolds-averaged Navier–Stokes and k-ω turbulence model equations, Computers & Fluids 34 (4) (2005) 507–540. https://doi.org/10.1016/j.compfluid.2003.08.004

[5] Bijl, H., Carpenter, M., Vatsa, V., Time integration schemes for the unsteady Navier-Stokes equations, Proceedings of the 15th AIAA Computational Fluid Dynamics Conference, Anaheim, American Institute of Aeronautics & Astronautics, 2001, pp. 1–11 (AIAA 2001-2612). https://doi.org/10.2514/6.2001-2612

[6] Bruno, O. P., Cubillos, M., Higher-order in time "quasi-unconditionally stable" ADI solvers for the compressible Navier–Stokes equations in 2D and 3D curvilinear domains, Journal of Computational Physics 307 (2016) 476–495. https://doi.org/10.1016/j.jcp.2015.12.010

[7] Bruno, O. P., Cubillos, M., On the quasi-unconditional stability of BDF-ADI solvers for the compressible Navier-Stokes equations and related linear problems, SIAM Journal on Numerical Analysis 55 (2) (2017) 892–922. https://doi.org/10.1137/15M1042279

[8] Calvo, M. P., de Frutos, J., Novo, J., An efficient way to avoid the order reduction of linearly implicit Runge-Kutta methods for nonlinear IBVP's, Modeling, Simulation, and Optimization of Integrated Circuits, Basel, Birkhäuser Basel, 2003, pp. 321–332. https://doi.org/10.1007/978-3-0348-8065-7_20

[9] Cash, J. R., Diagonally implicit Runge-Kutta formulae with error estimates, IMA Journal of Applied Mathematics 24 (3) (1979) 293–301. https://doi.org/10.1093/imamat/24.3.293

[10] Cockburn, B., Lazarov, R., Gopalakrishnan, J., Unified hybridization of discontinuous Galerkin, mixed, and continuous Galerkin methods for second order elliptic problems, SIAM Journal on Numerical Analysis 47 (2) (2009) 1319–1365. https://doi.org/10.1137/070706616

[11] Cockburn, B., Shu, C. W., The local discontinuous Galerkin method for time-dependent convection-diffusion systems, SIAM Journal on Numerical Analysis 35 (6) (1998) 2440–2463. https://doi.org/10.1137/S0036142997316712

[12] Ding, H., Shu, C., Yeo, K. S., Xu, D., Numerical simulation of flows around two circular cylinders by mesh-free least square-based finite difference methods, International Journal for Numerical Methods in Fluids 53 (2) (2007) 305–332. https://doi.org/10.1002/fld.1281

[13] Franciolini, M., Fidkowski, K. J., Crivellini, A., Efficient discontinuous Galerkin implementations and preconditioners for implicit unsteady compressible flow simulations, Computers & Fluids 203 (2020) 1–18. https://doi.org/10.1016/j.compfluid.2020.104542

[14] Hairer, E., Nørsett, S. P., Wanner, G., Solving ordinary differential equations I. – Nonstiff problems, Springer-Verlag, Berlin Heidelberg, 1993.

[15] Kang, S., Characteristics of flow over two circular cylinders in a side-by-side arrangement at low Reynolds numbers, Physics of Fluids 15 (9) (2003) 2486–2498. https://doi.org/10.1063/1.1596412

[16] Kennedy, C. A., Carpenter, M. H., Diagonally implicit Runge-Kutta methods for ordinary differential equations. A review, Technical report No. NASA/TM 2016-219173, NASA Langley Research Center, 2016.

[17] Ketcheson, D. I., Seibold, B., Shirokoff, D., Zhou, D., DIRK schemes with high weak stage order, In: Spectral and High Order Methods for Partial Differential Equations ICOSAHOM 2018, Lecture Notes in Computational Science and Engineering, Springer Cham, 2020, pp. 453–463. https://doi.org/10.1007/978-3-030-39647-3_36

[18] Liang, C., Premasuthan, S., Jameson, A., High-order accurate simulation of low-Mach laminar flow past two side-by-side cylinders using spectral difference method, Computers & Structures 87 (11) (2009) 812–827. https://doi.org/10.1016/j.compstruc.2008.12.016

[19] Meneghini, J., Saltara, F., Siqueira, C., Ferrari, J., Numerical simulation of flow interference between two circular cylinders in tandem and side-by-side arrangements, Journal of Fluids and Structures 15 (2) (2001) 327–350. https://doi.org/10.1006/jfls.2000.0343

[20] Nguyen, N. C., Peraire, J., Cockburn, B., An implicit high-order hybridizable discontinuous Galerkin method for linear convection-diffusion equations, Journal of Computational Physics 228 (9) (2009) 3232–3254. https://doi.org/10.1016/j.jcp.2009.01.030

[21] Nguyen, N. C., Peraire, J., Cockburn, B., An implicit high-order hybridizable discontinuous Galerkin method for nonlinear convection-diffusion equations, Journal of Computational Physics 228 (23) (2009) 8841–8855. https://doi.org/10.1016/j.jcp.2009.08.030

[22] Rangarajan, A., May, G., Dolejsi, V., Adjoint-based anisotropic hp-adaptation for discontinuous Galerkin methods using a continuous mesh model, Journal of Computational Physics 409 (2020) 1–23. https://doi.org/10.1016/j.jcp.2020.109321

[23] Rosales, R. R., Seibold, B., Shirokoff, D., Zhou, D., Spatial manifestations of order reduction in Runge-Kutta methods for initial boundary value problems, 2019, ArXiv:1712.00897. https://doi.org/10.48550/arXiv.1712.00897

[24] Schütz, J., May, G., An adjoint consistency analysis for a class of hybrid mixed methods, IMA Journal of Numerical Analysis 34 (3) (2014) 1222–1239. https://doi.org/10.1093/imanum/drt036

[25] Schütz, J., Woopen, M., May, G., A combined hybridized discontinuous Galerkin/hybrid mixed method for viscous conservation laws, Hyperbolic Problems: Theory, Numerics, Applications (2012) 915–922.

[26] Verwer, J. G., Convergence and order reduction of diagonally implicit Runge-Kutta schemes in the method of lines, Numerical analysis (1986) 220–237.

[27] Wanner, G., Hairer, E., Solving ordinary differential equations II. – Stiff and differential-algebraic problems, Springer-Verlag, Berlin Heidelberg, 1996.

[28] Williamson, C. H. K., Three-dimensional aspects and transition of the wake of a circular cylinder, In: Turbulent Shear Flows 7, Springer Berlin Heidelberg, 1991, pp. 173–194. https://doi.org/10.1007/978-3-642-76087-7_14

[29] Woopen, M., Balan, A., May, G., A unifying computational framework for adaptive high-order finite element methods, Proceedings of the 22nd AIAA Computational Fluid Dynamics Conference, Dallas, American Institute of Aeronautics & Astronautics, 2015, pp. 1–22. https://doi.org/10.2514/6.2015-2601